Long-term sensory deprivation selectively rearranges functional inhibitory circuits in mouse barrel cortex

Peijun Li[a], Uwe Rudolph[b], and Molly M. Huntsman[a,1]

[a]Department of Pharmacology, Georgetown University Medical Center, Washington, DC 20057; and [b]Laboratory of Genetic Neuropharmacology, McLean Hospital, and Department of Psychiatry, Harvard Medical School, Belmont, MA 02478

Edited by Edward G. Jones, University of California, Davis, CA, and approved May 18, 2009 (received for review January 29, 2009)

Long-term whisker removal alters the balance of excitation and inhibition in rodent barrel cortex, yet little is known about the contributions of individual cells and synapses in this process. We studied synaptic inhibition in four major types of neurons in live tangential slices that isolate layer 4 in the posteromedial barrel subfield. Voltage-clamp recordings of layer 4 neurons reveal that fast decay of synaptic inhibition requires α1-containing $GABA_A$ receptors. After 7 weeks of deprivation, we found that $GABA_A$-receptor-mediated inhibitory postsynaptic currents (IPSCs) in the inhibitory low-threshold-spiking (LTS) cell recorded in deprived barrels exhibited faster decay kinetics and larger amplitudes in whisker-deprived barrels than those in nondeprived barrels in age-matched controls. This was not observed in other cell types. Additionally, IPSCs recorded in LTS cells from deprived barrels show a marked increase in zolpidem sensitivity. To determine if the faster IPSC decay in LTS cells from deprived barrels indicates an increase in α1 subunit functionality, we deprived α1(H101R) mutant mice with zolpidem-insensitive α1-containing $GABA_A$ receptors. In these mice and matched wild-type controls, IPSC decay kinetics in LTS cells were faster after whisker removal; however, the deprivation-induced sensitivity to zolpidem was reduced in α1(H101R) mice. These data illustrate a change of synaptic inhibition in LTS cells via an increase in α1-subunit-mediated function. Because α1 subunits are commonly associated with circuit-specific plasticity in sensory cortex, this switch in LTS cell synaptic inhibition may signal necessary circuit changes required for plastic adjustments in sensory-deprived cortex.

interneurons | networks | plasticity

Synaptic inhibition is involved in sensory processing at the very first stage of cortical integration in layer 4 of the rodent primary somatosensory (barrel) cortex (1). Both feedforward and feedback inhibition from local circuit inhibitory neurons regulates the integration of thalamic and intracortical inputs (2, 3). Inhibitory neurons are distinguished from each other by action potential firing properties, morphology, and biochemical expression (4, 5). Cortical inhibitory neurons are largely separated into two functional circuits that are thought to carry out two intertwined yet separate functions in sensory processing (6). Fast-spiking (FS) cells are either basket cells or chandelier cells and express parvalbumin (4). They are readily activated by thalamic afferents and are the primary mediator of thalamocortical feedforward inhibition, and recurrent synaptic inhibition onto FS cells is very fast (6, 7). Low-threshold-spiking (LTS) cells express varying combinations of somatostatin, vasoactive intestinal peptide, and cholecystokinin (4), are weakly activated by thalamic afferents, and contribute to intracortical inhibitory transmission, and recurrent synaptic inhibition onto LTS cells decays slowly (7, 8).

In cortex and other regions, an emerging feature in brain networks is the "$GABA_A$-specific circuit" (9). This circuit has three main components: (*i*) the type of presynaptic inhibitory neuron, (*ii*) the subcellular location of the postsynaptic contact (e.g., soma and dendrite), and (*iii*) the subunit composition of postsynaptic $GABA_A$ receptors at those locations (9–12). For example, α1-subunit-containing $GABA_A$ receptors contribute to fast synaptic currents, are positioned in somatic locations, and are often the postsynaptic target of parvalbumin-containing FS basket cells (9). Therefore, in circuits where feedforward inhibition is required to ensure the temporal fidelity of the postsynaptic response, the fast currents through somatically located α1-containing $GABA_A$ receptors are proposed to allow the postsynaptic neuron to detect coincident responses from convergent excitatory afferents (13). In mouse visual cortex, only α1-subunit-containing $GABA_A$-specific circuits were associated with controlling the onset of the critical period for ocular dominance shifts after monocular deprivation (14). This does not occur with pharmacological enhancement of synaptic inhibition using the α1-selective agonist zolpidem in α1(H101R) knockin mice (14, 15).

In the present study, we performed whole-cell recordings to differentiate synaptic inhibition among the four most common neurons in layer 4 of mouse barrel cortex. Using a combined pharmacologic and genetic approach, we found that inhibitory postsynaptic current (IPSC) decay depends largely on the presence of α1 subunit expression. To understand the role of $GABA_A$-specific circuits after long-term deprivation, we measured synaptic inhibition in all cell types from whisker-trimmed mice. We found that whisker removal increased the amplitude and sped up the decay rates of spontaneous IPSCs in LTS cells. To determine if subunit composition was responsible for this change in decay, we recorded from whisker-trimmed α1(H101R) knockin mice and wild-type controls and tested for the increased presence of α1 subunits with zolpidem. In both α1(H101R) and wild-type controls, whisker trimming resulted in faster IPSC decay in LTS cells. In addition, IPSCs in LTS neurons became highly sensitive to zolpidem in wild-type controls and insensitive to zolpidem in α1(H101R) knockin mice. Taken together, these data suggest that long-term whisker deprivation rearranges inhibitory circuits through the emergence of α1 subunit function at inhibitory synapses in LTS cells. This represents changes for the postsynaptic $GABA_A$ receptor configuration in a type of neuron that is normally not identified with the classic $GABA_A$-specific circuit required for plasticity.

Results

Cortical Neurons Are Differentially Distributed across Barrel Subregions. Whole-cell patch-clamp recordings of visually identified cortical neurons were performed from layer 4 tangential slices in adult mice. We recorded from a total of 278 cortical neurons in C57BL/6J, α1(H101R), and wild-type [α1(H101)] control mice and measured synaptic and intrinsic properties of the four most prevalent neurons in the barrels of the posteromedial barrel subfield (PMBSF) that correspond to the main mystacial whiskers (Fig. 1). Layer 4 neurons were categorized using biochemical markers and multiple physio-

Author contributions: M.M.H. designed research; P.L. and M.M.H. performed research; U.R. contributed new reagents/analytic tools; P.L. analyzed data; and P.L., U.R., and M.M.H. wrote the paper.

The authors declare no conflict of interest.

This article is a PNAS Direct Submission.

Freely available online through the PNAS open access option.

[1]To whom correspondence should be addressed. E-mail: mh257@georgetown.edu.

This article contains supporting information online at www.pnas.org/cgi/content/full/0900922106/DCSupplemental.

www.pnas.org/cgi/doi/10.1073/pnas.0900922106

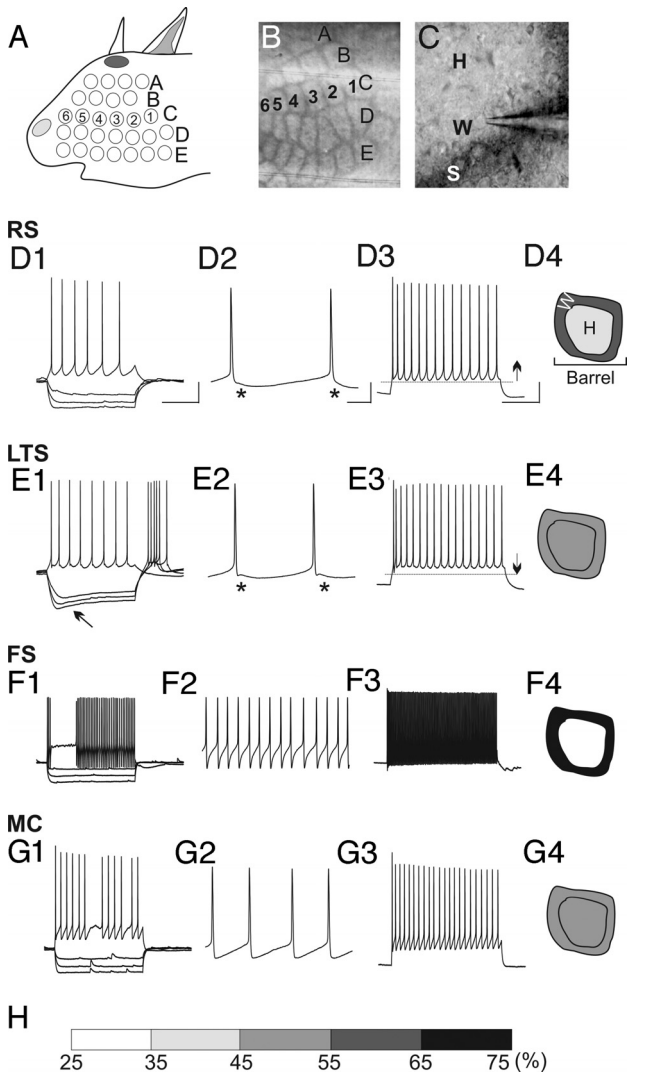

Fig. 1. Action potential firing properties and relative barrel position of cortical neurons in layer 4 tangential slices. (*A*) Schematic drawing of whisker position on the face. (*B*) Low-magnification image of live tangential slice in the recording chamber. The letters A, B, C, D, and E refer to the barrel rows of the PMBSF. (*C*) High-magnification image of living tangential slice of barrel subfield shows the hollow (H), wall (W), and septa (S). (*D–G*) Action potential firing patterns of the four most common neuron cell types in layer 4. For all cells: column 1, subthreshold and threshold traces from hyperpolarizing and depolarizing current pulses; column 2, threshold trace; column 3, suprathreshold trace; column 4, schematic of the proportion of cells recorded in the walls and hollows of a barrel in the tangential slice. (*D1–D3*) Regular-spiking cell firing properties. (*E1–E3*) Low-threshold-spiking cell firing properties. These two cell types are differentiated from each other by action potential shape (* in *D2* and *E2*), by the positioning of the last afterhyperpolarization potential in suprathreshold traces (dotted lines, arrows in *D3* and *D4*), and prominent sag (arrow in *E1*). (*F1–F3*) Firing properties of a fast-spiking cell (FS). (*G1–G3*) Firing properties of a Martinotti cell. (*H*) Percentages of cell location in the different barrel compartments used to determine shading in column 4 for each cell type. (Scale bars: column 1, 20 mV, 200 ms; column 2, 20 mV, 25 ms; column 3, 20 mV, 100 ms.)

logical parameters including: input resistance (R_{in}), action potential (AP) firing rate, threshold of firing, shape of the afterhyperpolarization potential (AHP), and the presence of rebound bursting after hyperpolarizing pulses (Fig. S1, Fig. S2, and Table S1). As expected, the excitatory regular-spiking (RS) cell was the most common cell type recorded in the tangential slice (Fig. 1*D*). The three main types of inhibitory cells in the slice were categorized as LTS cells, FS cells, and Martinotti cells (MCs) (Fig. 1 *E–G*). Regular-spiking cells in layer 4 fell into two categories: regular spiking and others that stuttered at threshold pulses [RS_{st} (16)]. Both RS cell types had numerous spines on their dendrites and were never colocalized with somatostatin or parvalbumin. In layer 4, RS and LTS cells share some similarities in spiking behavior (6). To differentiate these cells, we compared the difference between the peak AHP after the first AP and the peak AHP of the last AP in a depolarizing train (6). In LTS cells, the peak AHP after the final AP is at a more depolarized level compared with the first (dotted line, Fig. 1*E3*) (6). Low-threshold-spiking cells were further set apart from all other neurons via R_{in} values, the size of the I_h current ("sag height") in hyperpolarizing pulses, and somatostatin expression ($n = 3$, Fig. S1*B*). Fast-spiking cells were grouped by high-frequency firing patterns, low R_{in} values, and parvalbumin expression ($n = 27$, Fig. S1*C*). Martinotti cells were somatostatin positive ($n = 7$, Fig. S1*D*) and fit into the physiologically defined "classic accommodating" group (5). Martinotti cells were distinguished from LTS cells (also somatostatin positive) by multiple biophysical criteria and AHP shape (Fig. 1*G2* and Fig. S2) The overall cellular distribution of neurons across the hollows and walls differed for each cell type. The RS cells, LTS cells, and MCs were differentially distributed across barrel walls and hollows. Most of the FS cells recorded in the tangential slice were positioned in barrel walls (walls, 67.1% vs. hollows, 32.9%; however a χ^2 test proved that this was not significant $P = 0.156$) (Fig. 1*F4*). On the basis of the cellular distribution of neurons that remain functional in the tangential slice, different zones appear to exist across barrel subregions (or cortical columns) in terms of inhibitory function.

Heterogeneous IPSCs in the Four Main Types of Layer 4 Neurons. To examine inhibitory function within the confines of a barrel, we measured biophysical properties of IPSCs of all neuron types (Fig. 2, *SI Text*, and Table S2). We found that IPSC decay kinetics of layer 4 cortical neurons were heterogeneous. In a previous study, LTS cells in layer 5 were shown to have slow IPSC decay kinetics that differed from those of fast-decaying FS cells (7). In LTS and FS cells in layer 4, we observe this same pattern, with FS representing the fastest weighted decay ($\tau_{d,w}$) times ($\tau_{d,w} = 4.55 \pm 0.26$ ms, $n = 19$) and LTS cells representing slowest decay kinetics of layer 4 neurons ($\tau_{d,w} = 10.95 \pm 0.69$ ms, $n = 12$). Thus, these two functional circuits maintain similarities in synaptic function from layer to layer. Inhibitory postsynaptic currents in RS cells ($\tau_{d,w} = 8.40 \pm 0.43$ ms, $n = 11$) and MCs ($\tau_{d,w} = 6.35 \pm 0.18$ ms, $n = 5$) exhibited intermediate decay.

Long-Term Whisker Deprivation Alters Synaptic Inhibition in LTS Neurons. Because the barrels of the PMBSF retain their shapes in the tangential slice, visually identifying neurons in individual barrels in whisker-deprived animals is possible. To determine the effects of sensory deprivation on synaptic inhibition, we chronically trimmed the first four whiskers in rows D and E from the contralateral snout starting at postnatal day 7 (P7) and lasting for 7 weeks (Fig. 3 *A–D*). This time frame was chosen because of previous deprivation studies that illustrated changes in whisker response properties and $GABA_A$ receptor binding (17, 18). Cytochrome oxidase (CO) histochemistry performed on select slices after physiological recordings verified decreased neuronal activity in deprived barrels (Fig. 3 *C* and *D*) (19).

We measured differences in IPSC decay kinetics between neurons in barrels corresponding to trimmed whiskers and those corresponding to intact whiskers in control mice in the four main types of neurons in layer 4. Compared with IPSCs recorded from nondeprived mice, we did not observe major differences in intrinsic or synaptic inhibition from RS cells, FS cells, or MCs (Table S2). In contrast, the largest impact of sensory deprivation was observed in LTS cells, where IPSC decay time was significantly decreased by 28% compared with those of age-matched controls (Fig. 3 *E–I*). Inhibitory postsynaptic currents in LTS cells from deprived barrels

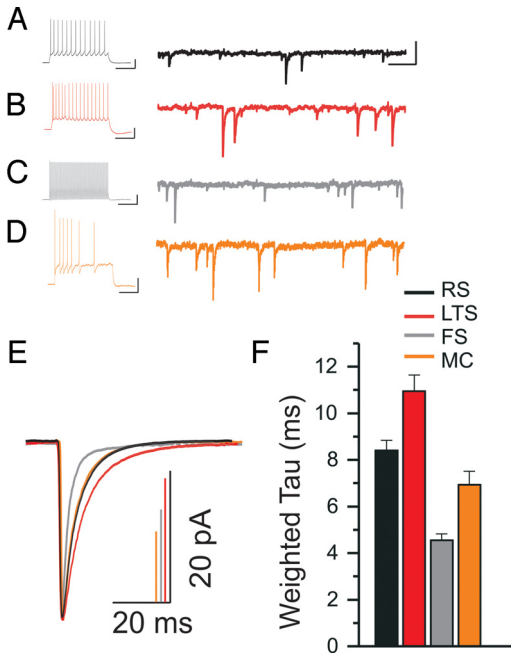

Fig. 2. Layer 4 cortical neurons display unique inhibitory postsynaptic currents (IPSC) decay kinetics. (*A*) Current-clamp recording showing firing behavior of a regular-spiking (RS) cell from a depolarizing current pulse. To the right is the voltage-clamp recording of the cell representing a continuous raw trace of IPSCs spanning 2 s. (*B–D*) Current-clamp and voltage-clamp recordings for: a low-threshold-spiking (LTS) cell, a fast-spiking (FS) cell, and a burst accommodating Martinotti cell (MC), respectively. [Scale bars: for the current-clamp traces, 20 mV, 200 ms; for the voltage-clamp traces, 50 pA, 200 ms.] (*E*) Isolated IPSCs from cells in *A–D* (in matching colors to the recordings above) were collected and averaged into a single trace (RS, $n = 188$; LTS, $n = 173$; FS, $n = 161$; MC, $n = 89$). Amplitudes of all averaged IPSCs were scaled to illustrate decay differences. All averaged IPSC traces were fit with a double-exponential decay function, and then weighted time constant ($\tau_{d,w}$) values were derived from these fits. (*F*) Mean values of $\tau_{d,w}$ from pooled data of all cells in each neuron category.

were considerably faster than the characteristic slowly decaying IPSCs recorded in nondeprived mice (deprived, $\tau_{d,w} = 7.95 \pm 0.38$ ms, $n = 9$; nondeprived, $\tau_{d,w} = 10.95 \pm 0.69$ ms, $n = 12$; $P = 0.0026$). A similar decrease was noted for half-width values (deprived, 4.66 ± 0.18 ms, $n = 9$; nondeprived, 8.68 ± 0.88 ms, $n = 12$; $P = 0.0009$). In addition to decay kinetics, we observed an increase in IPSC amplitude for LTS cells in whisker-deprived barrels (deprived, 51.68 ± 10.22 pA, $n = 9$; nondeprived, 28.03 ± 4.5 pA, $n = 12$; $P = 0.032$) (Fig. 3*J*). However, we did not see alterations in rise time or frequency. In data gathered from age-matched controls (using high-chloride electrodes), we report a small but significant increase in firing frequency in LTS cells from deprived barrels (39.3 ± 2.7 Hz, $n = 9$) versus nondeprived (31.1 ± 2.3 Hz, $n = 12$; $P = 0.033$) but no changes in other intrinsic properties.

Alterations in the decay kinetics of IPSCs are likely dependent on many factors, such as the composition of synaptic $GABA_A$ receptors. In cortical neurons, fast decay of IPSCs requires $\alpha 1$ subunits (7). $\alpha 1$(H101R) knockin mice (on the C57BL/6J background) have a point mutation in the $\alpha 1$ subunit at a conserved histidine located in the benzodiazepine site on all benzodiazepine-sensitive α subunits. This switch to the arginine residue renders $\alpha 1$-containing receptors insensitive to classical benzodiazepines and the imidazopyridine zolpidem. If $\alpha 1$ subunits are involved in IPSC decay kinetics, then there should be prolongation of IPSCs by zolpidem in wild-type C57BL/6J mice and no effect in $\alpha 1$(H101R) knockin mice. For all cell types, except LTS cells, zolpidem enhances IPSC decay (Fig. S3 and Table S3). To determine if $\alpha 1$ subunits are responsible for deprivation-induced decreases in IPSC decay kinetics in LTS cells, we whisker-trimmed $\alpha 1$(H101R) knockin and wild-type mice (Fig. 4 and Table S4). In both $\alpha 1$(H101R) and wild-type mice, IPSCs in LTS cells showed a decrease in the time course of decay (wild type, $\tau_{d,w} = 7.46 \pm 0.44$ ms; $\alpha 1$(H101R), $\tau_{d,w} = 7.38 \pm 0.35$ ms) after deprivation. Additionally, and in contrast to nondeprived animals, IPSC decay in LTS cells from deprived barrels was significantly slowed by zolpidem ($\tau_{d,w} = 9.95 \pm 0.43$ ms, $n = 9$; $P = 0.0008$) in wild-type mice (Fig. 4 *A* and *C*). This deprivation-induced slowing of IPSCs by zolpidem in wild-type mice was not observed in LTS cells from whisker-deprived $\alpha 1$(H101R) knockin mice ($\tau_{d,w} = 8.15 \pm 0.40$ ms, $n = 6$; $P = 0.18$; Fig. 4 *B* and *C*), indicating significant contribution of functional $\alpha 1$ subunits.

Discussion

With a combined pharmacologic and genetic approach, our primary findings suggest that prolonged sensory deprivation triggers a remodeling of inhibitory synapses on LTS inhibitory neurons. We compared biophysical characteristics of spontaneous IPSCs recorded from layer 4 neurons and examined the effects of long-term sensory deprivation on these characteristics. The specific findings are as follows: (*i*) inhibitory neurons are unevenly distributed across barrel subdivisions in the PMBSF, (*ii*) the biophysical properties of $GABA_A$-receptor-mediated IPSC decay kinetics differ among physiologically identified layer 4 neurons, (*iii*) cells with fast-decaying IPSCs contain functional $\alpha 1$ subunits, whereas LTS cells in nondeprived barrels have slow decay kinetics and little to no $\alpha 1$ subunit function, (*iv*) in LTS cells selectively, long-term sensory deprivation speeds IPSC decay and increases the amplitude of IPSCs. This alteration of IPSC decay is accompanied by an increased sensitivity to zolpidem, and further experiments indicate that this phenomenon is mediated through an increase in $\alpha 1$ subunit functionality.

Differential Distribution of Neurons across the Hollow and Wall Indicate Functional Zones within a Barrel. Although the primary location of the cell bodies of GABA neurons is within barrel walls (20, 21), our results show that there is differential neuron distribution across barrel subregions (Fig. 1). The majority of FS cells are located in walls, but LTS cells and MCs are distributed somewhat evenly across both the hollow and the wall of a barrel. What does this distribution indicate about possible distinct functional zones within a barrel? Even though cell density is higher in the barrel walls (22) and combined immunohistochemical staining for 2-deoxyglucose and glutamic acid decarboxylase indicates that inhibitory neurons are more reactive to whisker activity than their excitatory counterparts (23), the walls are less reactive to CO (19). On the basis of the present findings, the higher density of FS cells in the walls appears to signify that this subregion consists of a more homogenous population of cells performing related functions such as providing feedforward inhibition (24). Conversely, the central hollow of a barrel is made up of a heterogeneous group of neurons that are likely performing different thalamocortical and intracortical whisker-activated functions (6, 25). Therefore, the metabolically active subregions revealed by CO staining signify distinct functional zones (17), and these zones are based on the differential positioning of physiologically distinct neurons across a barrel column.

Long-Term Sensory Deprivation Causes a Switch in Functional Synaptic $GABA_A$ Receptors Expressed on LTS Cells. Location and pharmacological sensitivity indicate subunit-specific contributions to IPSC biophysics. Although there are multiple factors that determine decay time course—including the GABA transient, uptake mechanisms, or even the structure of presynaptic terminals (26–28)—the stochastic nature of ion channels formed by different $GABA_A$ receptor subunits expressed is also a factor. Many studies point to the correlation between fast synaptic events and high $\alpha 1$ subunit expression as evidence of this association (7, 29–31), and in the

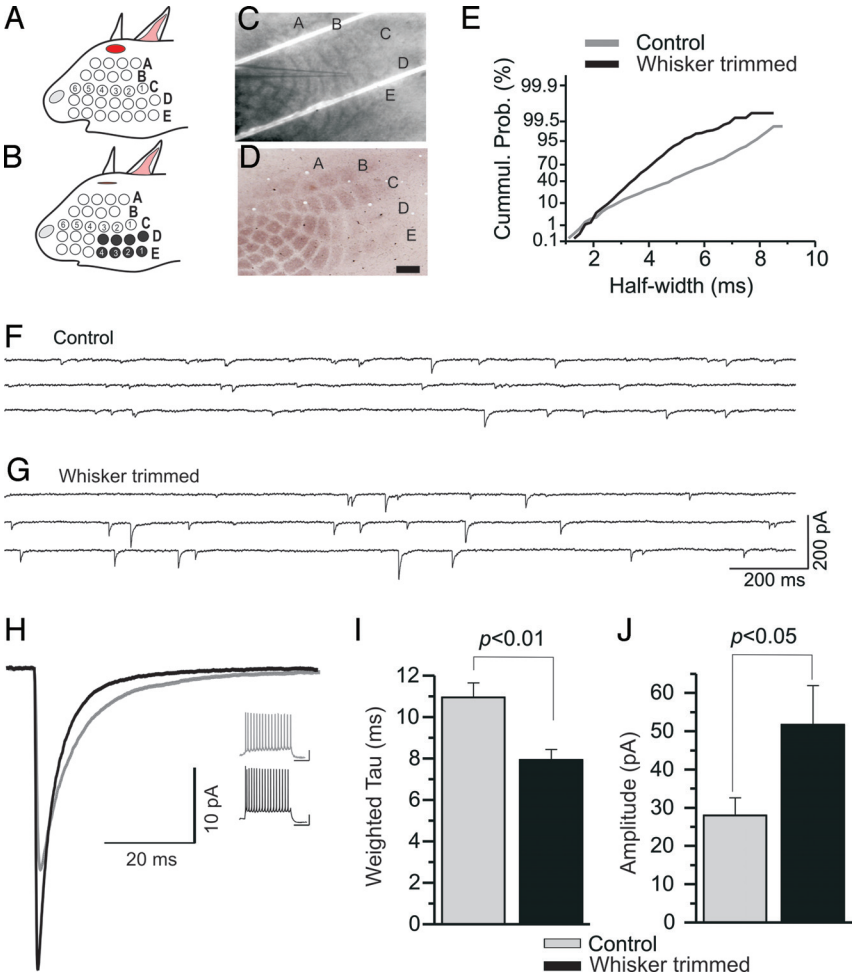

Fig. 3. Sensory deprivation reduces synaptic decay kinetics in low-threshold-spiking (LTS) neurons. (*A* and *B*) Schematics of whisker trimming showing the first 4 whiskers of the D and E rows were removed. (*C* and *D*) Image of a tangential slice from a deprived mouse in a recording chamber (*C*) and the same slice resectioned/processed for cytochrome oxidase (CO) (*D*). [Scale bar: 500 μm.] Note the reduction of reaction product for CO in the barrels corresponding to trimmed whiskers. (*E*) Cumulative probability histogram of half-width distribution of inhibitory postsynaptic currents (IPSCs) from an LTS cell in a control mouse (gray) and an LTS cell in a whisker-trimmed mouse (black). The use of a nonlinear scale illustrates the relative distributions of events within the recording period. (*F* and *G*) Representative raw traces of IPSCs from an LTS cell in a control mouse (*F*) and an LTS cell from a deprived barrel from a whisker-trimmed mouse (*G*). (*H*) Superimposed averaged IPSC traces from the two LTS cells in *F* (gray trace, $n = 203$ events) and *G* (black trace, $n = 142$ events) with corresponding current-clamp traces on the right control mouse (gray) and the deprived mouse (black). [Scale bar: 20 mV, 200 ms.] Histograms of mean values for $\tau_{d,w}$ (*I*) and amplitude (*J*).

present study, we show that layer 4 cortical neurons with relatively fast IPSC decay rates contain the α1 subunit in postsynaptic $GABA_A$ receptors (Fig. 2 and Fig. S2). Additionally, we and others show that a characteristic feature of synaptic inhibition in LTS cells is the slow decay of $GABA_A$-receptor-mediated IPSCs (7). We further show that these cells likely do not have a large degree of α1 subunit function in their IPSCs and indicate that IPSCs in LTS cells are likely originating from an α subunit other than an α1 subunit. In barrel cortex, α1 and α2 subunits are the two main $GABA_A$ receptor subunits expressed in layer 4 (32). In particular, α1 subunits are expressed at high levels in barrel walls (32), matching the distribution of FS cells and fast IPSC decay kinetics. In contrast, α2 subunits are equally expressed in both the walls and the hollows (32, 33), likely reflecting the distribution of slower-decaying LTS cells.

Remarkably and unexpectedly, we show that long-term whisker deprivation causes a speeding of decay and an increase in the amplitude of IPSCs in LTS cells, suggestive of a possible increase in α1 subunit function (Fig. 3). This is further supported by the increased zolpidem sensitivity in these neurons (34). Importantly, this zolpidem sensitivity does not occur in α1(H101R) mice, indicating that this increased sensitivity is mediated by the increased functionality specifically of α1 subunits in IPSCs in these cells. The imidazopyridine zolpidem binds at the benzodiazepine site and is often used for its selectivity to slow the decay rates of IPSCs from neurons that express α1-containing $GABA_A$ receptors (7, 30). However, in addition to its high potency at α1-containing $GABA_A$ receptors, it also has a moderate potency at α2- and α3-containing $GABA_A$ receptors and is thus not absolutely α1-specific (35). Questions remain as to the cause of increased α1 function. One possibility could be changes in $GABA_A$ receptor subunits that result in a subunit switch in postsynaptic receptors. Data pertaining to subunit changes are conflicting. Long-term whisker removal decreases muscimol binding (18), yet decreasing activity in barrels does not seem to affect α1 subunit expression (36). However, sensory deprivation can cause an increase in benzodiazepine sensitivity in the mouse visual system (37, 38). There is possibly a switch of synaptic $GABA_A$ subunits in LTS cells from a majority of α2-containing receptors to α1 via a homeostatic up-regulation of α1 subunits (as noted by amplitude increases) or a down-regulation of α2 subunits (as noted by decay decreases). Although we show an increase in α1 function, data from the present study indicate that possible changes may involve alterations that do not involve changes in expression levels, such as phosphorylation (39). A major redistribution of α1 subunits from synaptic to extrasynaptic locations on the cell membrane appears unlikely, because we observed no significant changes in rise times (40). Our finding of increased α1 subunit functionality does not rule out additional contributions to altered IPSC properties through presynaptic mechanisms, such as altered structure of presynaptic terminals or the selective loss of specific types of presynaptic inhibitory neurons (12, 40–45). Interestingly, we do not observe changes in IPSCs in RS cells from whisker-deprived mice (42). However, this may be due to different deprivation times and recording conditions.

Are Specific Inhibitory Networks Required for Cortical Plasticity? A role for inhibitory neurotransmission in plasticity is by no means a new idea (46). In sensory cortex GABA neurons, synapses and

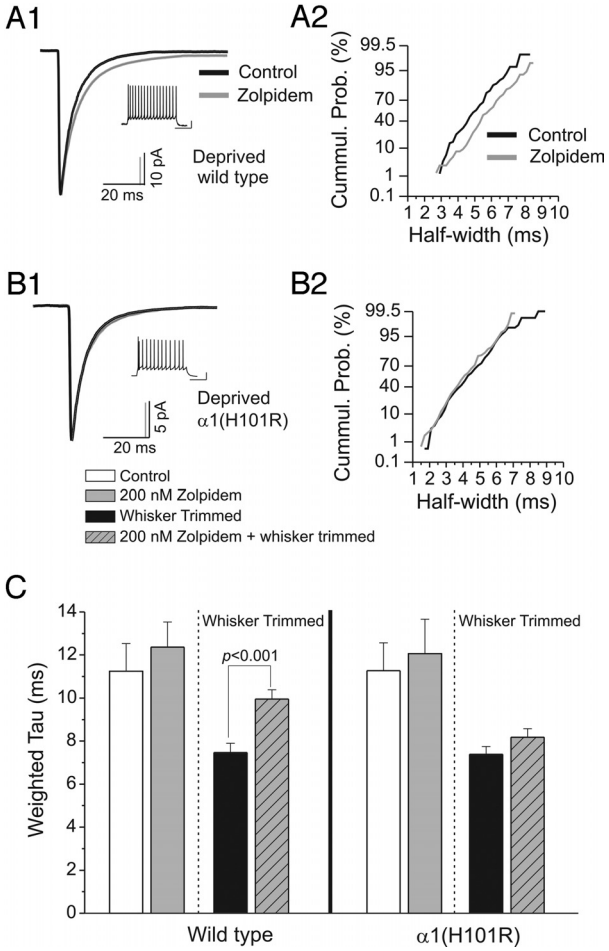

Fig. 4. Inhibitory circuit remodeling depends upon increased α1 subunit function. (*A1*) Averaged inhibitory postsynaptic current (IPSC) traces from a whisker-deprived wild-type C57BL/6J mouse in artificial cerebral spinal fluid (ACSF; black, n = 81 events) and in zolpidem–ACSF (gray, n = 75 events). (*A2*) Cumulative distribution plot of IPSC half-width (using a nonlinear scale for the y axis) from the cell in *A1* during ACSF (black) and zolpidem application (gray). (*B1*) Averaged IPSC traces from a deprived α1(H101R) knockin mouse in ACSF (black, n = 206 events) and during zolpidem (gray, n = 166 events). (*B2*) Cumulative distribution plot of IPSC half-width from cell in *B1* during ACSF (black) and zolpidem application (gray). (*C*) Histogram of pooled values of $\tau_{d,w}$ derived from fitted IPSCs from low-threshold-spiking cells recorded from wild-type (*Left*) and α1(H101R) (*Right*) knockins. The hatched lines separate nondeprived from whisker-trimmed mice. Note that the deprivation-induced enhancement of IPSC decay in wild-type mice is eliminated in α1(H101R) mice.

$GABA_A$ receptors are altered by sensory deprivation (18, 47–49). However, the concept of specialized inhibitory circuits involving specific GABA neurons and defined $GABA_A$ receptor subtypes in precise cellular locations has only recently emerged. $GABA_A$-specific circuits are likely mediators of plastic changes in sensory cortex in developing and early postnatal development (14, 42, 50). For example, $GABA_A$-specific circuits involving postsynaptic α1 subunits (and not α2 subunits) appear to be able to speed the onset of the critical period (14). There is also evidence showing that inhibitory neurotransmission is critical for the developmental maturation of neurons (51) and the absence of inhibition at critical times in development may underlie dysfunction in diseases such as autism (52). Data from the present study show that long-term deprivation periods trigger a switch in α1-subunit-mediated inhibition in an inhibitory neuron that is not typically associated with fast α1-mediated inhibition (7). Does this switch in functional inhibition on LTS cells signify an attempt to create a novel $GABA_A$-specific circuit? If so, what would a change of only a few milliseconds contribute to overall cortical function in deprived sensory cortex? Even though LTS neurons are only a fraction of the overall inhibitory neuronal population, the output of inhibition from this particular type of neuron may yield wide reaching effects at the network level. Changes in decay kinetics, even on the millisecond timescale, can alter the synchronization of large populations of neurons (53, 54), particularly if fast decay from α1 subunits is involved (55). Thus, as our result of increased firing frequency in LTS cells shows, even subtle changes in recurrent inhibition onto LTS cells may result in significant consequences such as observed in basket cell development (56). The fact that this change occurs on LTS cells is especially significant. Low-threshold-spiking cells are interconnected to each other through electrical synapses and are readily recruited into synchronous activation via metabotropic glutamatergic transmission (8, 57). Presumably, LTS cell synchrony could have wide ranging effects on excitatory neuron firing. Low-threshold-spiking neurons are weakly activated by thalamic afferents and are considered to be more involved in intracortical rather than thalamocortical inhibitory transmission (6). Therefore, alterations in recurrent inhibition onto LTS cells may account for increased cell synchrony observed in nondeprived barrels (58). Consequently, deprivation may require a new $GABA_A$-specific circuit that involves increased α1-subunit-mediated function in LTS cells for the repositioning of sensory maps after deprivation.

Materials and Methods

In Vitro Slice Preparation. All experiments were carried out in accordance with approved procedures (Georgetown University, 07-073). Control mice (C57BL/6J; The Jackson Laboratory), gene-targeted mice [α1(H101R)], and wild-type control mice [α1(H101) from the C57BL/6J strain] of either sex (P21-P49) were used. Mice were deeply anesthetized with carbon dioxide until unresponsive to tail or toe pinch. Brains were removed, blocked, and placed in an ice-cold-oxygenated slicing solution for 2 min containing 234 mM sucrose, 11 mM glucose, 24 mM $NaHCO_3$, 2.5 mM KCl, 1.25 mM $NaH_2PO_4{\cdot}H_2O$, 10 mM $MgSO_4$, and 0.5 mM $CaCl_2$. To isolate layer 4 of the primary somatosensory cortex, the brain was blocked at a simultaneous 30° angle in the horizontal plane and a 10° angle in the anterior–posterior plane. Slices were then sectioned at 200 μm and incubated for 1 h in preheated (32 °C), oxygen-equilibrated standard artificial cerebral spinal fluid (ACSF; 126 mM NaCl, 26 mM $NaHCO_3$, 10 mM glucose, 2.5 mM KCl, 1.25 mM $NaH_2PO_4{\cdot}H_2O$, 2 mM $MgCl_2{\cdot}6H_2O$, and 2 $CaCl_2{\cdot}2H_2O$; pH 7.4). Slices were visualized with a fixed-stage, upright microscope (Nikon) equipped with a 4× objective and a 60× insulated objective, IR illumination, and an IR-sensitive video camera (COHU).

Electrophysiological Recording Procedures. Whole-cell patch-clamp recordings were obtained from visually identified neurons. Recordings were made at room temperature (21–23 °C) to allow for more accurate analysis of IPSC decay and retains the health of slices from older animals. Brief suction pulses generated from a solenoid-controlled vacuum transducer were applied to break into the cell and establish whole-cell configuration. Voltage- and current-clamp recordings were obtained using a Multiclamp amplifier (700A; Molecular Devices) and digitized with a DigiData (1322A; Molecular Devices). The intracellular pipette solution contained high chloride to enhance the driving force of IPSCs (70 mM K-gluconate, 70 mM KCl, 2 mM NaCl, 10 mM Hepes, and 4 mM EGTA, pH 7.3, corrected with KOH; 290 mOsM). In some cases, biocytin was added to the pipette solution for posthoc morphological and biochemical characterization (Fig. S1). Inhibitory postsynaptic currents were recorded from barrel cortex neurons in voltage-clamp mode held at −60 mV. Inhibitory postsynaptic currents were measured at a sampling rate of 125 μs intervals (8 kHz) and filtered at 2 kHz. To measure the short time frame of rise times (the time measured from the start of an event to the peak ≈0.5–1.5 ms), a sampling rate of 50 μs (20 kHz) and 10 kHz filtering were required. At this rate, IPSCs were accurately sorted by slow versus fast rise times, and we only compared IPSCs under a threshold of rise time duration not to exceed 1.5 ms. Spontaneous $GABA_A$-receptor-mediated IPSCs were isolated by applying 6,7-dinitroquinoxaline-2,3-dione (20 μM DNQX, Tocris) and (+/−)-2-amino-5-phosphonopentanoic acid (100 μM APV, Tocris). Zolpidem (200 nM; Tocris) was bath applied.

We used two different analysis programs [Clampfit, version 9.2, and Detector (J. R. Huguenard, Stanford University)] to measure action potential

firing patterns and IPSC decay kinetics. Isolated IPSCs were aligned and averaged into a single averaged event. Double-exponential fits of baseline-subtracted averaged inhibitory events were made with the offset forced to zero. The decay of averaged IPSCs from peak to baseline is based on the double-exponential function:

$$f(t) = A_{fast}e^{-t/\tau fast} + A_{slow}e^{-t/\tau slow}. \quad [1]$$

Fitted IPSCs were used to determine the weighted time constant:

$$\tau_{d,w} = [(A_{fast}\ \tau_{fast}) + (A_{slow}\ \tau_{slow})]/(A_{fast} + A_{slow}). \quad [2]$$

Data were analyzed with Origin, version 6.0 (MicroCal Software), and statistical significance was measured using both independent and paired *t* tests and χ^2 tests.

Sensory Deprivation. Whiskers were trimmed under light anesthesia (isoflurane) starting at P7. The first four whiskers from rows D and E were trimmed, leaving the remaining three rows (A, B, and C) intact and repeated every 2–3 days (Fig. 3*B*) After ≈7–8 weeks of trimming, recordings were made from the contralateral hemisphere from whisker-trimmed mice in deprived barrels and compared with age-matched controls. Cytochrome oxidase histochemistry was used to verify deprived barrels in acute slices. Sections were rinsed in two washes of phosphate buffer (0.1 M). In a small flask, 20 mg of diaminobenzidine (Sigma) was mixed in 36 mL of phosphate buffer and filtered. Then, 1.6 g of sucrose and 16 mg of cytochrome *c* (Sigma) were added. Sections were incubated at 37 °C for 2 h, then rinsed, mounted on subbed slides, and covered with a cover slip.

ACKNOWLEDGMENTS. We thank Esther Krook-Magnuson for critical reading of this manuscript. This work was supported by National Institutes of Health Grant NS053719 (to M.M.H.).

1. White EL, Rock MP (1981) A comparison of thalamocortical and other synaptic inputs to dendrites of two non-spiny neurons in a single barrel of mouse SmI cortex. *J Comp Neurol* 195:265–277.
2. Thomson AM, West DC, Hahn J, Deuchars J (1996) Single axon IPSPs elicited in pyramidal cells by three classes of interneurones in slices of rat neocortex. *J Physiol* 496:81–102.
3. Agmon A, Connors BW (1992) Correlation between intrinsic firing patterns and thalamocortical synaptic responses of neurons in mouse barrel cortex. *J Neurosci* 12:319–329.
4. Markram H, et al. (2004) Interneurons of the neocortical inhibitory system. *Nat Rev Neurosci* 5:793–807.
5. Wang Y, et al. (2004) Anatomical, physiological and molecular properties of Martinotti cells in the somatosensory cortex of the juvenile rat. *J Physiol* 561:65–90.
6. Beierlein M, Gibson JR, Connors BW (2003) Two dynamically distinct inhibitory networks in layer 4 of the neocortex. *J Neurophysiol* 90:2987–3000.
7. Bacci A, Rudolph U, Huguenard JR, Prince DA (2003) Major differences in inhibitory synaptic transmission onto two neocortical interneuron subclasses. *J Neurosci* 23:9664–9674.
8. Beierlein M, Gibson JR, Connors BW (2000) A network of electrically coupled interneurons drives synchronized inhibition in neocortex. *Nat Neurosci* 3:904–910.
9. Fritschy JM, Brunig I (2003) Formation and plasticity of GABAergic synapses: Physiological mechanisms and pathophysiological implications. *Pharmacol Ther* 98:299–323.
10. Klausberger T, Roberts JD, Somogyi P (2002) Cell type- and input-specific differences in the number and subtypes of synaptic $GABA_A$ receptors in the hippocampus. *J Neurosci* 22:2513–2521.
11. Nyiri G, Freund TF, Somogyi P (2001) Input-dependent synaptic targeting of α_2-subunit-containing $GABA_A$ receptors in synapses of hippocampal pyramidal cells of the rat. *Eur J Neurosci* 13:428–442.
12. Ali AB, Thomson AM (2008) Synaptic α5 subunit-containing $GABA_A$ receptors mediate IPSPs elicited by dendrite-preferring cells in rat neocortex. *Cereb Cortex* 18:1260–1271.
13. Pouille F, Scanziani M (2001) Enforcement of temporal fidelity in pyramidal cells by somatic feed-forward inhibition. *Science* 293:1159–1163.
14. Fagiolini M, et al. (2004) Specific $GABA_A$ circuits for visual cortical plasticity. *Science* 303:1681–1683.
15. Rudolph U, et al. (1999) Benzodiazepine actions mediated by specific γ-aminobutyric $acid_A$ receptor subtypes. *Nature* 401:796–800.
16. Krook-Magnuson EI, Li P, Paluszkiewicz SM, Huntsman MM (2008) Tonically active inhibition selectively controls feedforward circuits in mouse barrel cortex. *J Neurophysiol* 100:932–944.
17. Fuchs JL, Salazar E (1998) Effects of whisker trimming on $GABA_A$ receptor binding in the barrel cortex of developing and adult rats. *J Comp Neurol* 395:209–216.
18. Simons DJ, Land PW (1987) Early experience of tactile stimulation influences organization of somatic sensory cortex. *Nature* 326:694–697.
19. Land PW, Simons DJ (1985) Cytochrome oxidase staining in the rat SmI barrel cortex. *J Comp Neurol* 238:225–235.
20. Lin CS, Lu SM, Schmechel DE (1985) Glutamic acid decarboxylase immunoreactivity in layer IV of barrel cortex of rat and mouse. *J Neurosci* 5:1934–1939.
21. Chmielowska J, Stewart MG, Bourne RC, Hamori J (1986) γ-Aminobutyric acid immunoreactivity in mouse barrel field: A light microscopical study. *Brain Res* 368:371–374.
22. Woolsey TA, Van der Loos H (1970) The structural organization of layer IV in the somatosensory region (SI) of mouse cerebral cortex. The description of a cortical field composed of discrete cytoarchitectonic units. *Brain Res* 17:205–242.
23. McCasland JS, Hibbard LS (1997) GABAergic neurons in barrel cortex show strong, whisker-dependent metabolic activation during normal behavior. *J Neurosci* 17:5509–5527.
24. Gabernet L, Jadhav SP, Feldman DE, Carandini M, Scanziani M (2005) Somatosensory integration controlled by dynamic thalamocortical feed-forward inhibition. *Neuron* 48:315–327.
25. Tan Z, Hu H, Huang ZJ, Agmon A (2008) Robust but delayed thalamocortical activation of dendritic-targeting inhibitory interneurons. *Proc Natl Acad Sci USA* 105:2187–2192.
26. Barberis A, Lu C, Vicini S, Mozrzymas JW (2005) Developmental changes of GABA synaptic transient in cerebellar granule cells. *Mol Pharmacol* 67:1221–1228.
27. Thompson SM, Gahwiler BH (1992) Effects of the GABA uptake inhibitor tiagabine on inhibitory synaptic potentials in rat hippocampal slice cultures. *J Neurophysiol* 67:1698–1701.
28. Szabadics J, Tamás G, Soltesz I (2007) Different transmitter transients underlie presynaptic cell type specificity of $GABA_{A,slow}$ and $GABA_{A,fast}$. *Proc Natl Acad Sci USA* 104:14831–14836.
29. Vicini S, et al. (2001) $GABA_A$ receptor α1 subunit deletion prevents developmental changes of inhibitory synaptic currents in cerebellar neurons. *J Neurosci* 21:3009–3016.
30. Hollrigel GS, Soltesz I (1997) Slow kinetics of miniature IPSCs during early postnatal development in granule cells of the dentate gyrus. *J Neurosci* 17:5119–5128.
31. Huntsman MM, Huguenard JR (2000) Nucleus-specific differences in $GABA_A$-receptor-mediated inhibition are enhanced during thalamic development. *J Neurophysiol* 83:350–358.
32. Golshani P, Truong H, Jones EG (1997) Developmental expression of $GABA_A$ receptor subunit and GAD genes in mouse somatosensory barrel cortex. *J Comp Neurol* 383:199–219.
33. Paysan J, Kossel A, Bolz J, Fritschy JM (1997) Area-specific regulation of γ-aminobutyric acid type A receptor subtypes by thalamic afferents in developing rat neocortex. *Proc Natl Acad Sci USA* 94:6995–7000.
34. Kiss A, Soderman A, Bundzikova J, Pirnik Z, Mikkelsen JD (2006) Zolpidem, a selective $GABA_A$ receptor α_1 subunit agonist, induces comparable Fos expression in oxytocinergic neurons of the hypothalamic paraventricular and accessory but not supraoptic nuclei in the rat. *Brain Res Bull* 71:200–207.
35. Graham D, Faure C, Besnard F, Langer SZ (1996) Pharmacological profile of benzodiazepine site ligands with recombinant $GABA_A$ receptor subtypes. *Eur Neuropsychopharmacol* 6:119–125.
36. Penschuck S, Paysan J, Giorgetta O, Fritschy JM (1999) Activity-dependent regulation of $GABA_A$ receptors. *Ann NY Acad Sci* 868:654–666.
37. Madar I, Scheffel U, Frost JJ (1994) Transient increase in the in vivo binding of the benzodiazepine antagonist [^{3}H]flumazenil in deafferented visual areas of the adult mouse brain. *Synapse* 18:79–85.
38. Wang WF, et al. (2003) Adenosine A1 and benzodiazepine receptors and glucose metabolism in the visual structures of rats monocularly deprived by enucleation or eyelid suture at a sensitive period. *Jpn J Ophthalmol* 47:182–190.
39. Kittler JT, et al. (2008) Regulation of synaptic inhibition by phospho-dependent binding of the AP2 complex to a YECL motif in the $GABA_A$ receptor γ2 subunit. *Proc Natl Acad Sci USA* 105:3616–3621.
40. Zhang N, Wei W, Mody I, Houser CR (2007) Altered localization of $GABA_A$ receptor subunits on dentate granule cell dendrites influences tonic and phasic inhibition in a mouse model of epilepsy. *J Neurosci* 27:7520–7531.
41. Micheva KD, Beaulieu C (1995) Neonatal sensory deprivation induces selective changes in the quantitative distribution of GABA-immunoreactive neurons in the rat barrel field cortex. *J Comp Neurol* 361:574–584.
42. Jiao Y, Zhang C, Yanagawa Y, Sun QQ (2006) Major effects of sensory experiences on the neocortical inhibitory circuits. *J Neurosci* 26:8691–8701.
43. Bartley AF, Huang ZJ, Huber KM, Gibson JR (2008) Differential activity-dependent, homeostatic plasticity of two neocortical inhibitory circuits. *J Neurophysiol* 100:1983–1994.
44. Nusser Z, Sieghart W, Benke D, Fritschy JM, Somogyi P (1996) Differential synaptic localization of two major γ-aminobutyric acid type A receptor α subunits on hippocampal pyramidal cells. *Proc Natl Acad Sci USA* 93:11939–11944.
45. McRae PA, Rocco MM, Kelly G, Brumberg JC, Matthews RT (2007) Sensory deprivation alters aggrecan and perineuronal net expression in the mouse barrel cortex. *J Neurosci* 27:5405–5413.
46. Jones EG (1993) GABAergic neurons and their role in cortical plasticity in primates. *Cereb Cortex* 3:361–372.
47. Hendry SH, Jones EG (1986) Reduction in number of immunostained GABAergic neurones in deprived-eye dominance columns of monkey area 17. *Nature* 320:750–753.
48. Huntsman MM, Isackson PJ, Jones EG (1994) Lamina-specific expression and activity-dependent regulation of seven GABAA receptor subunit mRNAs in monkey visual cortex. *J Neurosci* 14:2236–2259.
49. Micheva KD, Beaulieu C (1995) An anatomical substrate for experience-dependent plasticity of the rat barrel field cortex. *Proc Natl Acad Sci USA* 92:11834–11838.
50. Hensch TK, Fagiolini M (2005) Excitatory-inhibitory balance and critical period plasticity in developing visual cortex. *Prog Brain Res* 147:115–124.
51. Mataga N, Mizuguchi Y, Hensch TK (2004) Experience-dependent pruning of dendritic spines in visual cortex by tissue plasminogen activator. *Neuron* 44:1031–1041.
52. Rubenstein JL, Merzenich MM (2003) Model of autism: Increased ratio of excitation/inhibition in key neural systems. *Genes Brain Behav* 2:255–267.
53. Huntsman MM, Porcello DM, Homanics GE, DeLorey TM, Huguenard JR Reciprocal inhibitory connections and network synchrony in the mammalian thalamus. *Science* 283:541–543.
54. Bartos M, Vida I, Frotscher M, Geiger JR, Jonas P (2001) Rapid signaling at inhibitory synapses in a dentate gyrus interneuron network. *J Neurosci* 21:2687–2698.
55. van Ooyen A, Bosman L, Brussaard A (2004) Influence of the decay time of GABAergic postsynaptic current on the spatial spread of network activity. *Neurocomputing* 58–60:291–295.
56. Doischer D, et al. (2008) Postnatal differentiation of basket cells from slow to fast signaling devices. *J Neurosci* 28:12956–12968.
57. Gibson JR, Beierlein M, Connors BW (1999) Two networks of electrically coupled inhibitory neurons in neocortex. *Nature* 402:75–79.
58. Cheetham CE, Hammond MS, Edwards CE, Finnerty GT (2007) Sensory experience alters cortical connectivity and synaptic function site specifically. *J Neurosci* 27:3456–3465.